Vol. 03, Iss. 2 (2025) 237-249, DOI: 10.61552/JME.2025.02.008

JME

Journal of Materials and Engineering

www.jme.aspur.rs

Research article

Structures, Wettability, and Corrosion Resistance of Annealed Platinum/Ruthenium/Nitrogen Co-Doped Diamond-like Carbon Nano-Composite Thin Film at Different Temperatures

Nay Win Khun[a,b,*], Erjia Liu[a]

[a]*School of Mechanical and Aerospace Engineering, Nanyang Technological University, 50 Nanyang Avenue, Singapore 639798, Singapore,*
[b]*Institute of Microelectronics and Optoelectronics, Faculty of Electronics and Information Technology, Warsaw University of Technology, Koszykowa 75, 00-662 Warszawa, Poland.*

Keywords:

DLC nano-composite
DC magnetron sputtering
Annealing
Structure
Wettability
Corrosion

* Corresponding author:

Nay Win Khun
E-mail: khunnaywin@gmail.com

Received: 21 June 2024
Revised: 15 July 2024
Accepted: 20 August 2024

A B S T R A C T

Platinum/ruthenium/nitrogen co-doped diamond-like carbon nano-composite thin film (Pt/Ru/N-DLCNC-TF) deposited on a silicon (Si) substrate via DC magnetron sputtering deposition was heat treated at different temperatures of 100–400 ˚C to investigate the effect of rapid thermal annealing temperature (RTAT) on its chemical, physical, and corrosion properties. Increasing the RTAT increased its surface segregation of PtRu aggregates and graphitization, which in turn resulted in its increased surface roughness and water contact angle. It had a certain improvement in corrosion resistance in a 0.5 M hydrochloric (HCl) solution with an increased RTAT to 200 ˚C but a decrease in corrosion resistance with a further increased RTAT to 400 ˚C. It is clear that there are apparent changes in the structure, surface roughness, water contact angle, and corrosion resistance of the annealed Pt/Ru/N-DLCNC-TF with different RTATs.

1. INTRODUCTION

An ideal micro-mold has a surface with low adhesion, high hardness, low friction, and excellent wear resistance [1]. A large ratio of surface area to volume of a micro-mold gives rise to its adhesion to molded products [1]. Silicon (Si) and steel micro-molds used for the fabrication of miniature micro-fludic devices have a short service life because of their high adhesion and friction [2,3]. It is necessary to improve their surface properties with potential coatings. Diamond-like carbon thin

films (DLC-TFs) are well known for possessing high hardness, low friction, high wear resistance, and chemical inertness [4,5]. Besides, they possess hydrophobic surfaces with low surface energy [6]. Therefore, DLC-TFs with these superior properties can be considered as potential protective coatings for micro-molds.

The rigid sp^3-bonded cross-linking structures of DLC-TFs cause them to have high stresses and thereby poor adhesion to underlying substrates [4,7,8]. For this reason, metals such as Ni, Ti, Fe, Cr, Mo, etc. or non-metals such as N, Si, F, etc. are incorporated in DLC matrixes to improve their adhesion to underlying substrates by reducing their residual stresses [4,7,8]. Bootkul et al. [9] found an improvement in the adhesion strength of DLC-TFs with N doping as a result of a decrease in their sp^3 content. Khun et al. [7] reported that co-incorporation of Pt, Ru, and N elements improved the adhesion of DLCNC-TFs to Si substrates.

Annealing heat treatment (AHT) is considered another possibility to improve the adhesion strength of DLC-TFs because it can release their residual stresses via their graphitization and structural relaxation [10-12]. However, AHT does not always have a positive effect on the adhesion strength of DLC-TFs because improper AHT can degrade the film adhesion strength via a thermal mismatch between the film and substrate [13,14]. AHT can also affect the chemical compositions and structures of DLC-TFs and thereby their surface energies, which in turn results in subsequent changes in their surface hydrophobicity and adhesion [10-14]. Yang et al. [15] studied the effect of AHT on the surface hydrophobicity of molds coated with various hard coatings. Zhao et al. [16] investigated the effect of AHT on the structures, water contact angles, surface roughness, and corrosion resistance of hydrogenated DLC-TFs by conducting their correlations with each other.

In addition to the surface adhesion of micro-molds, their possible corrosion should be taken into account because steel used in micro-molds is susceptible to corrosion even with moisture, and its surface corrosion alters its surface chemical and physical properties [17]. The corrosion resistance of DLC-TFs used as protective coatings for micro-molds has become an important topic for micro-mold applications. It was reported that doping of metals or non-metals improved the adhesion strength of DLC-TFs but degraded their corrosion resistance due to their degraded sp^3-bonded cross-linking structures [8]. Co-doping of metals and non-metals in DLC-TFs in order to produce DLCNC-TFs with intented properties of low residual stress and high adhesion strength induces their chemical compositions to be complicated with AHT, which affects their structural, physical, and corrosion properties [11,12,15]. It is therefore necessary to systematically investigate the effect of AHT on the chemical compositions, structures, water contact angles, and corrosion resistance of DLCNC-TFs in order to successfully apply AHT as a post-treatment.

In this study, the Pt/Ru/N-DLCNC-TF deposited on a Si substrate using a DC magnetron sputtering deposition system was heat treated via RTA at different RTATs of 100–400 ˚C. A systematic investigation on changes in its chemical composition and structure, surface roughness, water contact angle, and corrosion resistance with respect to RTAT was carried out by conducting its structure-property correlation, which has not been reported in the literature yet.

2. EXPERIMENTAL DETAILS

2.1 Sample preparation

A Pt/Ru/N-DLCNC-TF was deposited on a p-type Si (100) substrate by co-sputtering a graphite (99.999% C) target and a Pt50Ru50 (99.99%) target with DC powers of 52 W/in^2 and 2.5 W/in^2, respectively, for 120 min. During the film deposition, argon and nitrogen gases were introduced into the deposition chamber as working and reactive gases at 50 sccm and 1 sccm, respectively, via their mass flow controllers. The background pressure of the deposition chamber evacuated prior to the film deposition was 7.5×10^{-6} Torr. The film deposition pressure was 3×10^{-3} Torr. The substrate, rotated at 22 rpm, was applied with a substrate bias of -30 V.

The Pt/Ru/N-DLCNC-TF was annealed by a Jipelec Jetfirst 100 RT processor (Figure 1) at different RTATs of 100–400 ˚C for 2 min. The temperature ramping and cooling rates were 25 ˚C/s and 6 ˚C/s, respectively. The RTA was carried out in a nitrogen environment supplied by nitrogen gas at 2000 sccm.

Fig. 1. A photo of RTA processor used in this study.

2.2 Characterization

X-ray photoelectron spectroscopy (XPS, Kratos Axis Ultra) was employed to measure the surface chemical compositions and bonding configurations of the as-deposited and annealed Pt/Ru/N-DLCNC-TFs. The radiation source was a monochromatic Al Kα X-ray radiation (hυ = 1486.71 eV). The pass energy of 40 W was used for C 1s + Ru 3d, N 1s, and Pt 4f to measure the chemical compositions by integrating their core-level peaks.

Renishaw S2000 micro-Raman spectroscopy with a He-Ne laser of 632.8 nm was applied to investigate the amorphous structures of the as-deposited and annealed Pt/Ru/N-DLCNC-TFs. Highly ordered pyrolytic graphite (HOPG) was used as a reference material.

Digital Instruments S-3000 atomic-force-microscopy (AFM) operated in a tapping mode was used to scan the surface topographies of the as-deposited and annealed Pt/Ru/N-DLCNC-TFs in a scan size of 1 μm × 1 μm. Five random measurements on each film were carried out to average arithmetic average roughness, R_a, values.

The water contact angles of the as-deposited and annealed Pt/Ru/N-DLCNC-TFs were measured with a FTA200 system by applying droplets of distilled water to their surfaces. Five water contact angle measurements on each coating were randomly carried out to get an average water contact angle.

The corrosion resistance of the as-deposited and annealed Pt/Ru/N-DLCNC-TFs was examined in a 0.5 M HCl solution at a scan rate of 0.8 mV/s using an EG & G 263A potentiostat/galvanostat workstation with a flat cell kit, which contained a standard saturated calomel reference electrode (244 mV at 25 ˚C), a platinum counter mesh, and a working electrode. Their exposed area was a circle of 1 cm in diameter. Their corrosion potentials (E_{corr}) in mV and currents (I_{corr}) in μA were obtained by fitting their polarization curves. Then, their polarization resistance (R_p) values in kΩ were calculated from their I_{corr} and anodic (β_a) and cathodic (β_c) Tafel slopes (V/I-decade) according to the equation (1) [7,18]:

$$Rq = \frac{(\beta a \times \beta c)}{2.3 Icorr(\beta a + \beta c)} \quad (1)$$

3. RESULTS AND DISCUSSION

Figure 2 shows the surface chemical compositions of the as-deposited and annealed Pt/Ru/N-DLCNC-TFs at different RTATs. The Pt, Ru, and N contents of the as-deposited Pt/Ru/N-DLCNC-TF are 4.2, 5.1, and 6.6 at.%, respectively. The Ru content is higher than the Pt content because of the core-shell structure of PtRu aggregates, with an inner core enriched with Pt and an outer shell enriched with Ru, which is consistent with the previous reports in Refs. [7,19].

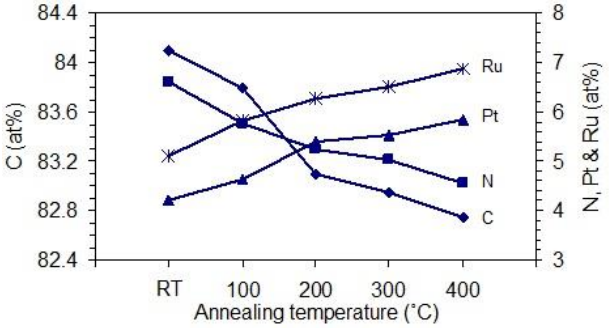

Fig. 2. Surface C, Pt, Ru, and N contents of as-deposited and annealed Pt/Ru/N-DLCNC-TFs at different RTATs.

In Figure 2, increasing the RTAT increases the surface Pt and Ru contents of the Pt/Ru/N-DLCNC-TF but decreases its surface N content so that its Pt and Ru contents at the RTAT of 400 ˚C are 5.8 at.% and 6.8 at.%, which are 38.1% and 33.3% higher than those of the one without the

RTA, while it has a 31.8% lower N content of 4.5 at.%. The Ru content is still higher than the Pt content for all the RTATs. The annealing induced structural relaxation enriches the film surface with PtRu aggregates due to the size effect of the Pt and Ru in the amorphous carbon structure [20,21]. The increased segregation of PtRu aggregates to the film surface associated with an increased RTAT contributes to the increased Pt and Ru contents [20,21]. Increases in the Pt and Ru fractions lead to a decrease in the N fraction, while the chemical inertness of the Pt and Ru elements with the N element is also responsible for the decreased N content [7].

Figure 3a shows the XPS C 1s + Ru 3d peaks of the as-deposited and annealed Pt/Ru/N-DLCNC-TFs at different RTATs, from which overlapping of the C 1s peak with the spin-orbit coupling peaks of Ru 3d(5/2,3/2) is found [7,22]. The C 1s peak of the as-deposited Pt/Ru/N-DLCNC-TF exists at a binding energy of about 284.9 eV, as increasing the RTAT to 400 ˚C shifts its binding energy to a lower value of about 284.6 eV as a result of its increased graphitization [7,11]. The C 1s peak of the as-deposited Pt/Ru/N-DLCNC-TF has a full-width-at-half-maximum (FWHM) of 1.88 eV, as its FWHM decreases to 1.65 eV with an increased RTAT to 400 ˚C, revealing a decrease in its bond angle and length disorders [4,23].

In Figure 3a, the XPS Ru 3d5/2 peak of the as-deposited Pt/Ru/N-DLCNC-TF exists at about 280.7 eV, as the increased RTAT to 400 ˚C shifts its binding energy to a lower value of about 280.4 eV, indicating the increased pure Ru rather than its oxides since the binding energy of a pure metal is lower than those of its oxides via an extra Coulombic interaction between photon emitted electrons and ion cores [7,22]. In Figure 3b, the spin-orbit coupling peaks of Pt 4f(7/2, 5/2) of the as-deposited Pt/Ru/N-DLCNC-TF at about 72 eV and 75.4 eV shift to lower binding energies of about 71.8 eV and 75.2 eV, respectively, with an increased RTAT to 400 ˚C as a result of the increased pure Pt with a lower binding energy. It is hypothesized that the RTA makes adsorbed surface O atoms gain more energy to break their bonds with surface Ru or Pt atoms and outgas as O2, as well as to react with weakly bonded C atoms and outgas as CO or CO2 [7,23]. These processes become more pronounced with an increased RTAT, so that the fraction of pure metals is higher with respect to their oxides with a higher RTAT.

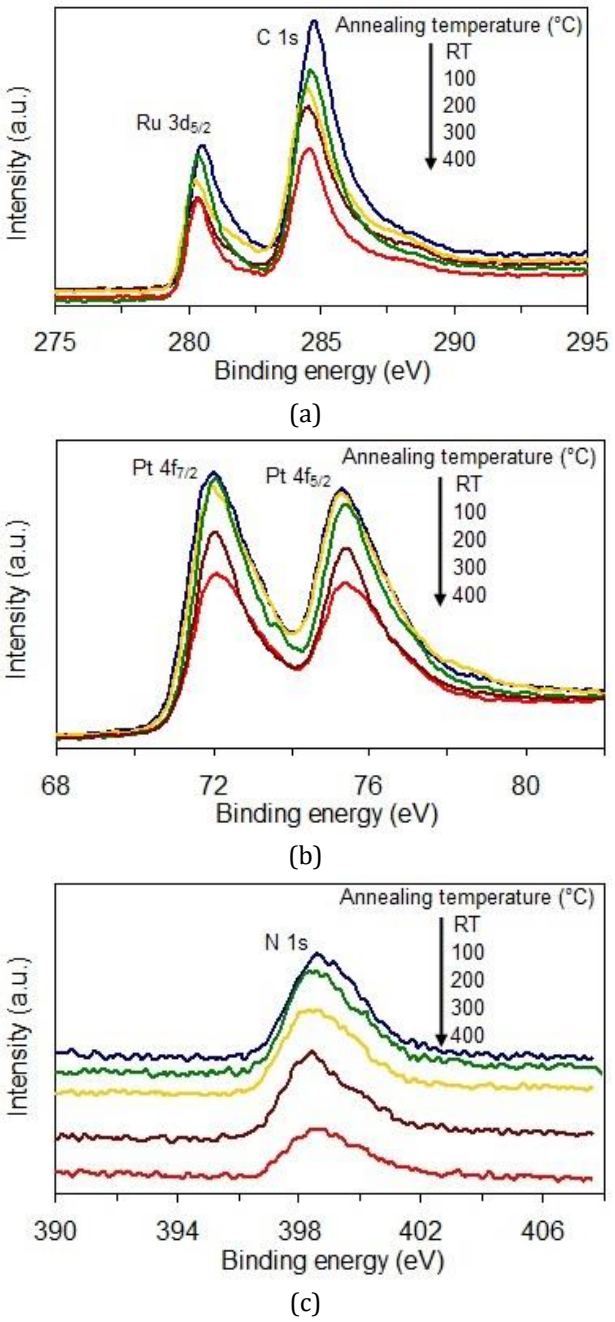

Fig. 3. XPS (a) C 1s + Ru 3d, (b) Pt 4f, and (c) N 1s peaks of as-deposited and annealed Pt/Ru/N-DLCNC-TFs at different RTATs.

Figure 3c shows the XPS N 1s peaks of the annealed Pt/Ru/N-DLCNC-TF at different RTATs. The N 1s peak of the as-deposited Pt/Ru/N-DLCNC-TF exists at a binding energy of about 398.8 eV, as its N 1s peak shifts to a lower binding energy of about 398.4 eV with an increased RTAT to 400 ˚C. The RTA of the Pt/Ru/N-DLCNC-TF results in its graphitization, which in turn changes the bonding configuration of N atoms from N-sp^3 to N-sp^2 and increases the number of N atoms in aromatic ring structures [4,7,18,24]. Therefore, the

increased number of N-sp^2 bonds with respect to N-sp^3 bonds shifts the N 1s peak to a lower binding energy [4,7,18,24].

The XPS Pt 4f and N 1s peaks were fitted using a Gaussian line shape and a Shirley background for the detailed analysis of their chemical bonding structures. The fitted XPS Pt 4f peaks of the as-deposited and annelaed Pt/Ru/N-DLCNC-TFs at 400 ˚C are shown in Figures 4a and 4b, respectively. They are deconvoluted into three spin-orbit coupling peaks: the Pt^0 peak at about 71.9 eV, the Pt^{2+} peak at about 73 eV, and the Pt^{4+} peak at about 74.6 eV in the Pt 4f7/2 region, indicating the neutral Pt and its oxides [7]. Increasing the RTAT develops the Pt^0 peak with respect to the Pt^{2+} and Pt^{4+} peaks, confirming the promoted pure Pt metal state, which is also true for Ru.

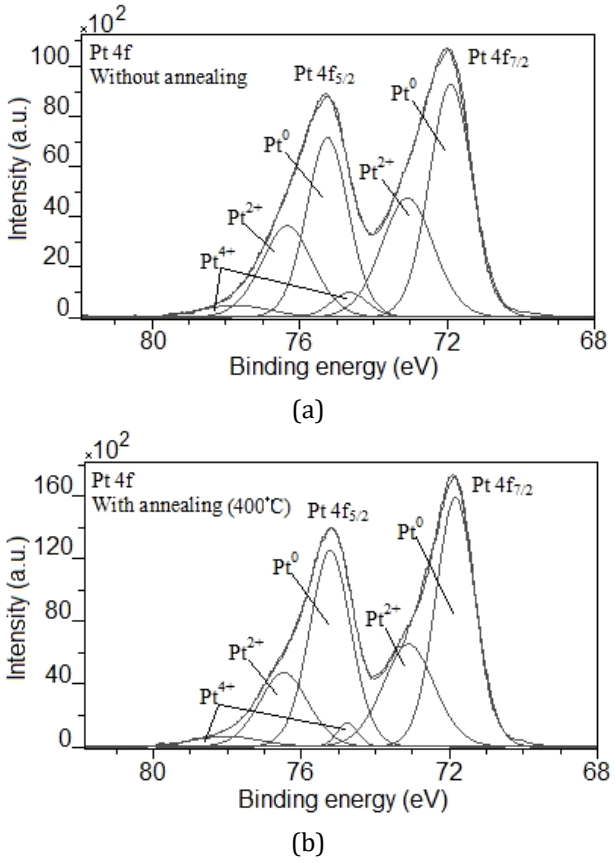

Fig. 4. Fitted XPS spin-orbit coupling peaks of Pt 4f(5/2,7/2) of (a) as-deposited and (b) annelaed Pt/Ru/N-DLCNC-TF at 400 ˚C.

Figures 5a and 5b show the fitted XPS N 1s peaks of the as-deposited and annealed Pt/Ru/N-DLCNC-TFs at 400 ˚C, respectively, which are deconvoluted into three peaks: the N-sp^2 peak at about 398.7 eV, the N-sp^3 peak at about 400.2 eV, and the N-O peak at about 402.5 eV [7,25,26]. Based on the comparison of their N-sp^2 and N-sp^3 peaks, the N-sp^2 peak develops with respect to the N-sp^3 peak with an increased RTAT, indicating the increased number of N atoms in not only sp^2 bonding configuration but also aromatic rings associated with the promoted graphitization of the amorphous carbon structure, although the intensity of the N 1s peak decreases with the decreased N content [4,7,25,26].

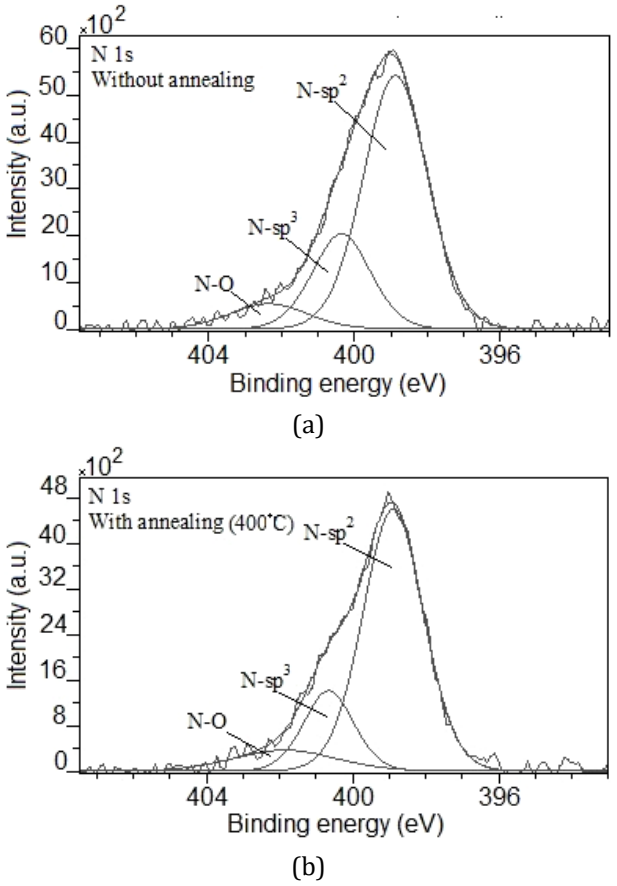

Fig. 5. Fitted XPS N 1s peaks of (a) as-deposited and (b) annelaed Pt/Ru/N-DLCNC-TFs at 400 ˚C.

Figure 6 shows the Raman spectra of the as-deposited and annealed Pt/Ru/N-DLCNC-TFs at different RTATs. The Raman spectrum of the HOPS has G and D peaks at 1580.1 cm^{-1} and 1334.6 cm^{-1}, respectively. The appearance of the D peak in the Raman spectrum of the HOPG indicates its disordered graphite structure [4]. The D peak is attributed to the breathing mode of sp^2 sites only in aromatic rings, as the stretching vibration of any pair of sp^2 sites in chains or aromatic rings is responsible for the G peak [4,7]. Since a typical Raman spectrum of the amorphous carbon structure is mainly

dominated by sp^2 sites rather than sp^3 sites, an increase in the intensity of the Raman spectrum shows an increase in the sp^2 fraction [4,7,18,27]. Therefore, the increased intensity of the Raman spectrum of the Pt/Ru/N-DLCNC-TF with an increased RTAT is indicative of its increased sp^2 fraction, while the portion of its Raman spectrum existing at about the D peak position of the HOPG develops, indicating the increased number of aromatic rings in its amorphous carbon structure via its increased graphitization.

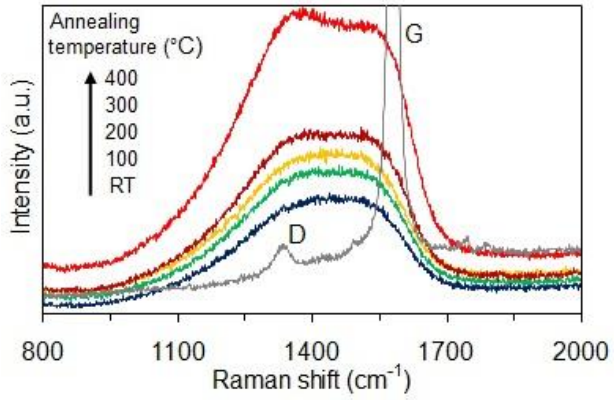

Fig. 6. Raman spectra of as-deposited and annealed Pt/Ru/N-DLCNC-TFs at different RTATs, and HOPG. Gray colored Raman spectrum with D and G peaks belongs to HOPG.

Figure 7a shows the fitted Raman spectrum of the as-deposited Pt/Ru/N-DLCNC-TF with two Gaussian G and D peaks and a linear background. The well-defined D and G peaks can be seen in its typical Raman spectrum, providing information about sp^2 bonds and aromatic rings in it since all sp^2 sites contribute to the G peak and the D peak is attributed to six-fold rings only [4].

Figure 7b shows the G peak positions of the Raman spectra of the as-deposited and annealed Pt/Ru/N-DLCNC-TFs at different RTATs. The G peak position of the as-deposited Pt/Ru/N-DLCNC-TF exists at about 1538.3 cm^{-1}. Increasing the RTAT to 400 ˚C shifts its G peak position to a larger value of about 1561.6 cm^{-1}. It was reported [4] that the disorder and loss of aromaticity weakened bonds and lowered vibrational density, which caused the G peak to shift downwards [4]. Beeman et al. [28] reported that a decrease in G peak position was attributed to bond angle disorder and a certain percentage of tetrahedral bonds. Therefore, the downward shift of the G peak with an increased RTAT can be correlated to the increased graphitization of the amorphous carbon structure, which increases the number of sp^2 bonds and aromatic rings and decreases not only the bond angle and length disorders but also the ring disorders.

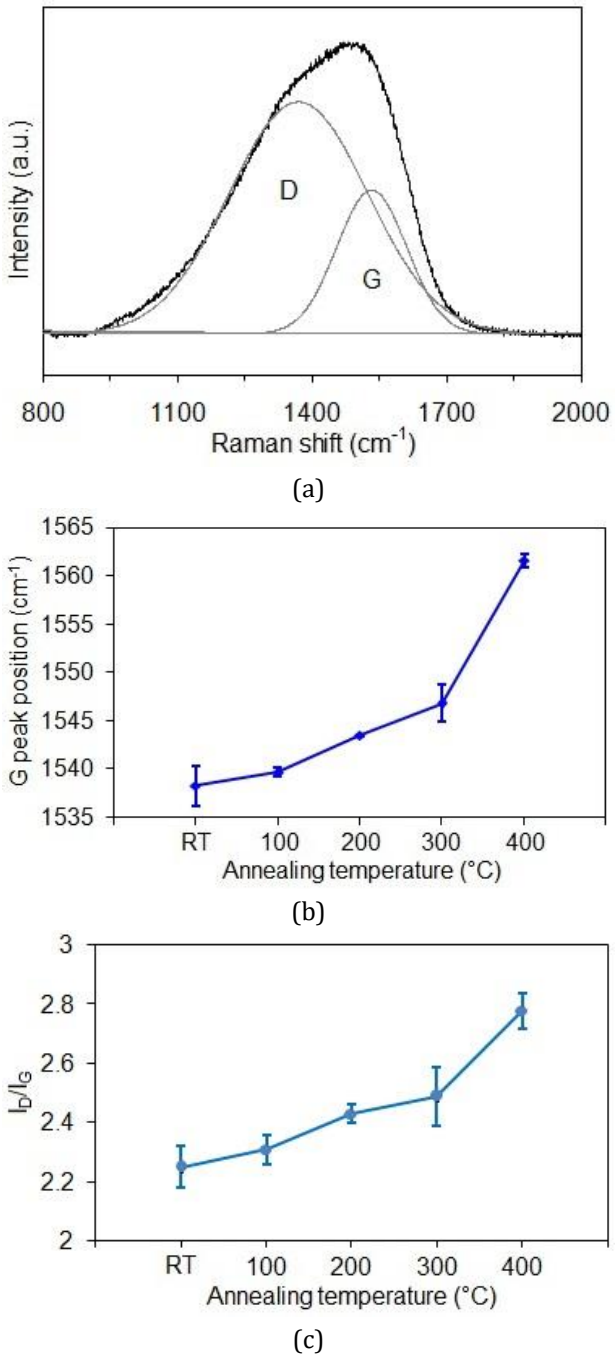

Fig. 7. (a) Fitted Raman spectrum of as-deposited Pt/Ru/N-DLCNC-TF. (b) G peak positions and (c) I_D/I_G ratios of Raman spectra of as-deposited and annealed Pt/Ru/N-DLCNC-TFs at different RTATs.

Figure 7c shows the I_D/I_G ratios of the Raman spectra of the as-deposited and annealed Pt/Ru/N-DLCNC-TFs at different RTATs. The I_D/I_G ratio of the as-deposited Pt/Ru/N-DLCNC-TF is 2.3, which means that it has a significant

number of aromatic rings. Increasing the RTAT increases its I_D/I_G ratio to 2.8, confirming its increased graphitization [4].

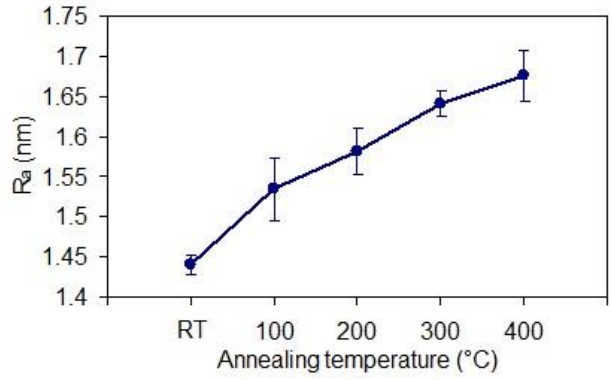

(a)

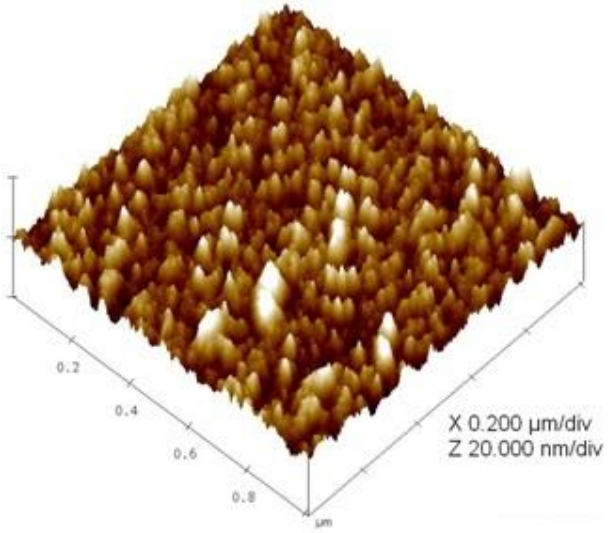

(b)

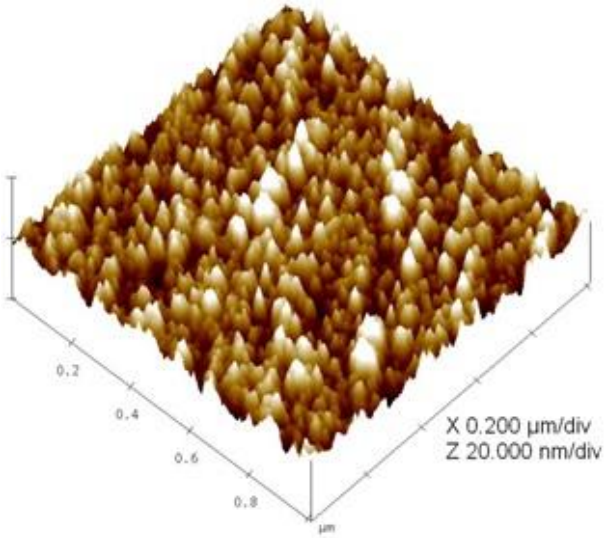

(c)

Figure 8: (a) R_a values of as-deposited and annealed Pt/Ru/N-DLCNC-TFs at different RTATs. AFM images showing surface topographies of (a) as-deposited and (b) annealed Pt/Ru/N-DLCNC-TF at 400 ˚C.

Figure 8a shows the Ra values of the as-deposited and annealed Pt/Ru/N-DLCNC-TFs at different RTATs. The Ra value of the as-deposited Pt/Ru/N-DLCNC-TF is about 1.4 nm, while its Ra value increases to about 1.7 nm (21.4% increase) with an increased RTAT to 400 ˚C. The increased segregation of PtRu aggregates to its surface with an increased RTAT is responsible for its increased surface roughness. Its increased sp^2 fraction or graphitic phases associated with its increased graphitization also give rise to its increased surface roughness by reducing its density [4,18,29].

The surface topographies of the as-deposited and annealed Pt/Ru/N-DLCNC-TFs at 400 ˚C are shown in Figures 8b and 8c, respectively. Although both surfaces have similar surface features, the annealed surface at 400 ˚C has a higher number of protruded surface asperities with a bright color, which are probably formed by the segregated PtRu aggregates or graphitic phases.

Figure 9a shows the water contact angles of the as-deposited and annealed Pt/Ru/N-DLCNC-TFs at different RTATs. The water contact angle of the as-deposited Pt/Ru/N-DLCNC-TF is about 78˚ (Figure 9b), as the increased RTAT to 400 ˚C results in its increased water contact angle to about 82.7˚ (6% increase) (Figure 9c). The wettability of the Pt/Ru/N-DLCNC-TF surface decreases with an increased RTAT. Carbon-nitrogen bonds associated with the incorporation of N atoms in the amorphous carbon structure enhance the surface polarity with attractive forces to react with polar water molecules [7,30,31]. Therefore, the decreased surface N content with an increased RTAT is responsible for the increased water contact angle of the Pt/Ru/N-DLCNC-TF by reducing the fraction of surface carbon-nitrogen bonds and weakening the surface polarity. Besides, the increased surface segregation of PtRu aggregates with an increased RTAT contributes to the increased water contact angle by decreasing the fraction of surface carbon-nitrogen bonds. Since C-O, Pt-O, and Ru-O bonds associated with adsorbed surface oxygen have strong polarities, the water contact angle of the Pt/Ru/N-DLCNC-TF should decrease with increased surface Pt and Ru contents [7,30,32]. However, its increased water contact angle indicates that its surface polarity is not influenced by its adsorbed surface oxygen in this

study because of the promoted pure metal states of the Pt and Ru elements rather than their oxides with an increased RTAT. The chemical inertness of the Pt and Ru elements is also responsible for the increased surface hydrophobicity with their increased contents [4]. Since air trapped in surface asperities below a water droplet can give rise to a large water contact angle, its increased surface roughness with an increased RTAT can be correlated to its increased water contact angle [19,33,34].

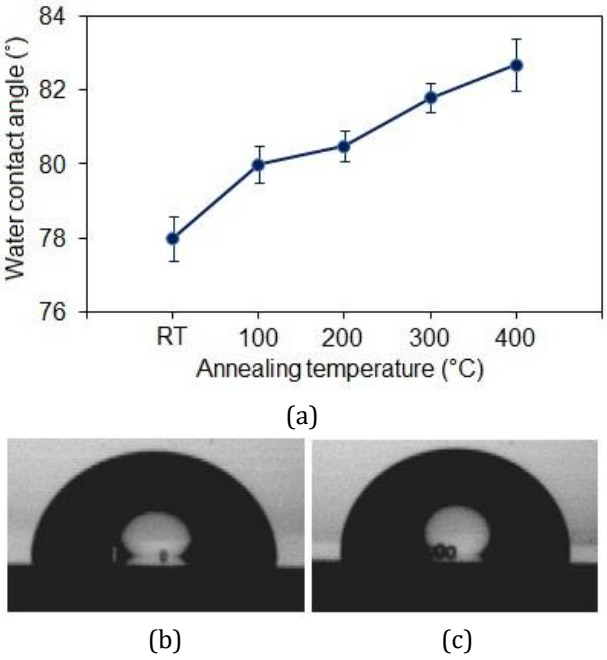

Fig. 9. (a) Water contact angles of as-deposited and annealed Pt/Ru/N-DLCNC-TFs at different RTATs. Water droplets on surfaces of (b) as-deposited and (b) annealed Pt/Ru/N-DLCNC-TFs at 400 ˚C.

The potentiodynamic polarization curves of the as-deposited and annealed Pt/Ru/N-DLCNC-TFs at different RTATs, measured in a 0.5 M HCl solution, are shown in Figure 9a. Their cathodic branches do not apparently change with RTAT, except for the one annealed at 200 ˚C. Their structural changes with different RTATs affect their anodic branches. A comparison of their potentiodynamic polarization currents shows that the annealed Pt/Ru/N-DLCNC-TF at 200 ˚C has the highest corrosion resistance among the samples used in this study.

The E_{corr} and R_p values of the as-deposited and annealed Pt/Ru/N-DLCNC-TFs at different RTATs are summarized in Figure 10b. The E_{corr} and R_p values of the as-deposited Pt/Ru/N-DLCNC-TF are -44 mV and 4.86 kΩ, respectively. Its E_{corr} value shifts to a more positive value of 335 mV (8.6 times higher) with an increased RTAT to 200 ˚C, while its R_p value increases to a larger value of 74 kΩ (15.2 times higher), indicating an increase in its corrosion resistance [7,18]. However, further increasing the RTAT to 400 ˚C turns to decrease its E_{corr} and R_p values to 40 mV (8.4 times lower) and 4.3 kΩ (17.2 times lower), respectively, as a result of a decrease in its corrosion resistance [7,18]. The R_p value of the annealed Pt/Ru/N-DLCNC-TF at 400 ˚C is 1.1 times lower than that of the one without the RTA, which means that the polarization resistance of the annealed Pt/Ru/N-DLCNC-TF at 400 ˚C in the HCl solution is not much lower than that of the as-deposited one.

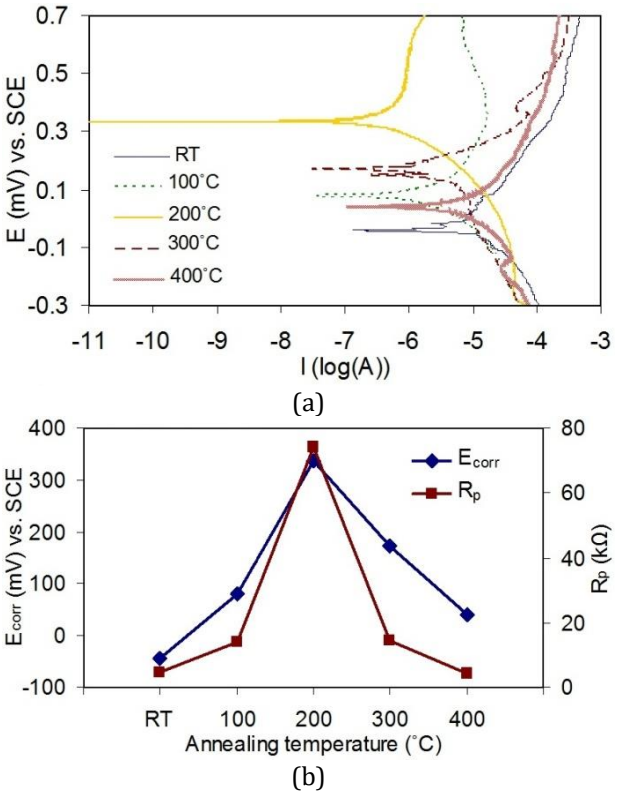

Fig. 10. (a) Potentiodynamic polarization curves and (b) corrosion parameters of as-deposited and annealed Pt/Ru/N-DLCNC-TFs at different RTATs, measured in a 0.5 M HCl solution.

The corrosion resistance of the Pt/Ru/N-DLCNC-TF is strongly influenced by its surface chemical composition since the surface is always first accessed by an electrolyte [8,11,18,35] The existence of Pt and Ru on the Pt/Ru/N-DLCNC-TF surface lessens its readily anodic dissolution in the HCl solution because Pt and Ru are electrochemically nobler than C [7,36]. It was reported that an increase in N content in the

amorphous carbon structure decreased its corrosion resistance because N doping, which induced the formation of new sp^2 sites as well as encouraged existing sp^2 sites to cluster, degraded its rigid sp^3-bonded cross-linking structure and thereby resulted in its readily anodic dissolution [4,18]. The decreased N content in the Pt/Ru/N-DLCNC-TF with an increased RTAT can be correlated to its increased corrosion resistance. High residual stress in the amorphous carbon structure can promote its susceptibility to corrosion in an aggressive electrolyte via film failure in terms of cracking and delamination on a microscale [37]. Besides, intrinsic structural defects (minute pores, imperfections, etc.) in the amorphous carbon structure negatively affect its corrosion resistance since corrosion always initiates at structural defects [7,18,38]. It is supposed that the RTA probably lessens the residual stress and intrinsic defects in the Pt/Ru/N-DLCNC-TF and thereby enhances its corrosion resistance. Therefore, the increased corrosion resistance of the Pt/Ru/N-DLCNC-TF in the HCl solution with an increased RTAT to 200 ˚C is attributed to its increased Pt and Ru contents, decreased N content, and reduced residual stress and structural defects.

Further increasing the RTAT to 400 ˚C through 200 ˚C, however, turns to decrease the corrosion resistance of the Pt/Ru/N-DLCNC-TF, as found in Figure 10b. It means that the Pt, Ru, and N contents of the Pt/Ru/N-DLCNC-TF no longer have an influence on its corrosion resistance beyond the RTAT of 200 ˚C. The hydrophilic surface is normally active in an aqueous electrolyte for corrosion, pointing out that there is no correlation between the promoted hydrophobicity of the Pt/Ru/N-DLCNC-TF surface and its increased corrosion [39]. The possible reason is that the increased surface segregation of PtRu aggregates above a certain critical level with an increased RTAT decreases the surface structural integrity of the Pt/Ru/N-DLCNC-TF, which leads to an increase in its readily anodic dissolution in the HCl solution. Weak interfaces between the PtRu aggregates and C matrix allow not only an easy attack of electrochemically active species (H^+, Cl^-, water molecules, etc.) to the film surface for anodic dissolution but also a permeation of an aggressive electrolyte into the film/substrate interface to attack it and cause the underlying Si substrate to dissolve, so that the increased surface Pt and Ru contents of the Pt/Ru/N-DLCNC-TF result in an increase in its corrosion by forming more surface networks of weak interfaces and degrading more its surface structural integrity [7,18,38]. Moreover, the degraded sp^3-bonded cross-linking structure of the Pt/Ru/N-DLCNC-TF associated with its graphitization should be correlated to its increased corrosion [7,18]. Furthermore, galvanic corrosion between the PtRu aggregates and C matrix becomes more severe with increased Pt and Ru contents or enhanced graphitization [7]. The enhanced electrical conductivity of the Pt/Ru/N-DLCNC-TF associated with its graphitization also encourages its anodic dissolution under applied voltages via faster electron transfer through it [7,18,38,40-42]. The influence of surface roughness on the corrosion of the Pt/Ru/N-DLCNC-TF should be taken into account because the higher surface roughness gives rise to a larger exposed area to an electrolyte for higher anodic dissolution as well as a higher number of surface atoms with the lack of a 3D coordination network with neighboring atoms to easily dissolve [43]. The increased surface roughness of the Pt/Ru/N-DLCNC-TF with an increased RTAT contributes to its increased corrosion. These combined effects lead to decreased corrosion resistance of the Pt/Ru/N-DLCNC-TF in the HCl solution by increasing the RTAT to more than 200 ˚C. Nevertheless, the corrosion resistance of the annealed Pt/Ru/N-DLCNC-TF at 400˚C is not much lower than that of the as-deposited one.

Figure 11a shows the surface morphology of the annelaed Pt/Ru/N-DLCNC-TF at 200 ˚C observed after its polarization measurement in a 0.5 M HCl solution, on which corrosion products are found, although any apparent corrosion damage is not found. The corrosion products, which resulted from electrochemical interaction between the film surface and HCl solution, probably lessen the corrosion current of the Pt/Ru/N-DLCNC-TF by blocking diffusion paths of electrochemically active species from the solution onto the film surface or into the underlying Si substrate and hindering their electrochemical reactions [7,18]. As a result, its anodic current does not apparently change with applied voltage, as found in the anodic branch of its polarization curve in Figure 10a.

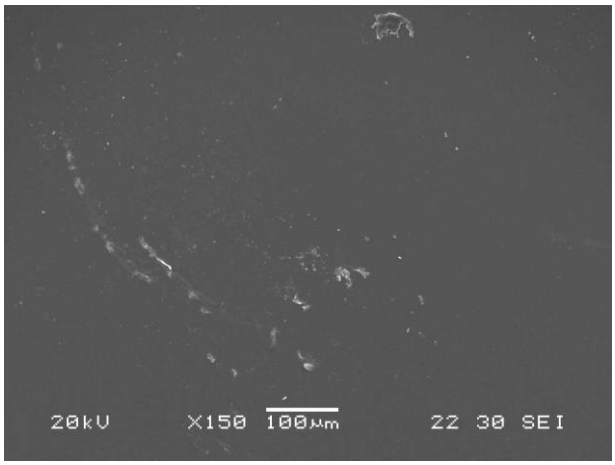

(a)

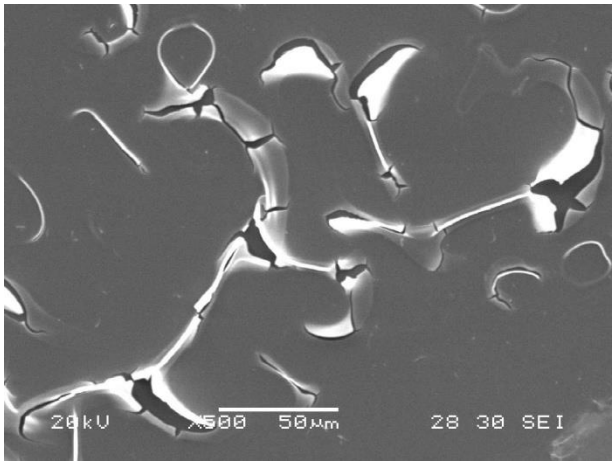

(b)

Fig. 11. Surface morphologies of annelaed Pt/Ru/N-DLCNC-TFs at (a) 200 ˚C and (b) 400 ˚C, observed after polarization measurements in a 0.5 M HCl solution.

Figure 11b shows the surface morphology of the annealed Pt/Ru/N-DLCNC-TF at 400 ˚C tested in the HCl solution, from which localized film delamination in micro-size is found. Electrochemically active species permeated through minute pores, pits, or weak interfaces between the PtRu aggregates and carbon matrix easily attack the film/substrate interface and subsequently cause undermining of the film. At the same time, galvanically induced corrosion occurring at the film/substrate interface due to the different electrochemical potentials between the film and substrate accelerates the film undermining process via the anodic dissolution of the interface [7,18,38,40-42]. As a result, a large volume of the HCl solution is allowed to access the undermined areas. Eventually, the tension of the solution accessed and corrosion products formed inside the undermined areas force the film off the substrate. With shifting the applied potential to more positive values, minute pores develop themselves as well as connect with neighboring pores to form micropores. The interconnection of micropores leads to the formation of a network, and the undermining of the film under micropores becomes more severe, resulting in localized film delamination, as found in Figure 11b, and contributing to the overall anodic current. Such a similar film delamination was found on the tested area of the as-deposited Pt/Ru/N-DLCNC-TF but with less severity [7]. Therefore, the anodic currents of the as-deposited and annleaed Pt/Ru/N-DLCNC-TFs at 400 ˚C apparently increase with an increased applied voltage (Figure 10a). There is no observation of the localized film delamination on the tested area of the annealed Pt/Ru/N-DLCNC-TF at 200 ˚C, probably due to its improved corrosion resistance and thereby its shorter anodic dissolution in the HCl solution (Figure 10a).

4. CONCLUSION

The effects of RTAT on the chemical composition and structure, surface roughness, water contact angle, and corrosion resistance of the annealed Pt/Ru/N-DLCNC-TF were systematically investigated.

- The surface Pt and Ru contents of the Pt/Ru/N-DLCNC-TF increased with an increased RTAT, while its surface N content decreased.
- The sp^2 friction of the Pt/Ru/N-DLCNC-TF increased with an increased RTAT as a result of its promoted graphitization.
- The increased surface segregation of PtRu aggregates and promoted graphitization of the Pt/Ru/N-DLCNC-TF with an increased RTAT resulted in its increased surface roughness, so that the Ra value at the RTAT of 400 ˚C was 21.4% larger than that without the RTA.
- The water contact angle of the Pt/Ru/N-DLCNC-TF increased with an increased RTAT due to its decreased contents of polar bonds and increased surface roughness, so that the water contact angle at the RTAT of 400 ˚C was 6 % larger than that without that RTA.

- The annealed Pt/Ru/N-DLCNC-TF at 200 ˚C had 15.2 times higher polarization resistance in a 0.5 M HCl solution than the as-deposited one, as the polarization resistance of the annealed Pt/Ru/N-DLCNC-TF at 400 ˚C was 18.2 times lower than that of the one annealed at 200 ˚C. It indicated that the Pt/Ru/N-DLCNC-TF had a certain improvement in its corrosion resistance in the HCl solution with an increased RTAT to 200 ˚C.
- The RTAT had an apparent influence on the chemical, physical, and corrosion properties of the annealed Pt/Ru/N-DLCNC-TF.

Acknowledgement

This work was supported by the research grant (EWI-0601-IRIS-035-00) from the Environment & Water Industry Development Council (EWI), Singapore.

REFERENCES

[1] B. Saha, E. Liu, S. B. Tor, N. W. Khun, D. E. Hardt and J.H. Chun, "Anti-sticking behavior of DLC coated silicon micro-molds," *Journal of Micromechanics and Microengineering*, vol. 19, pp. 105025–7, Sep. 2009, doi:10.1088/0960-1317/19/10/105025.

[2] X. R. Yan, T. Xu, S. S. Yue, H. W. Liu, Q. J. Xue and S. R. Yang, "Characterization of hydrogenated diamond-like carbon films electrochemically deposited on a silicon substrate," *Journal of Physics D: Applied Physics*, vol. 37, pp. 416–24, Aug. 2004, doi:10.1088/0022-3727/37/17/012.

[3] J. Narasimhan and I Papautsky, "Polymer embossing tools for rapid prototyping of plastic microfludic devices," *Journal of Micromechanics and Microengineering*, vol. 14, pp. 96–103, Oct. 2003, doi:10.1088/0960-1317/14/1/013.

[4] J. Robertson, "Diamond-like carbon amorphous," *Materials Science and Engineering: R: Reports*, vol. 37, iss. 4–6, pp. 129–281, May 2002. doi:10.1016/S0927-796X(02)00005-0.

[5] A. Grill, "Tribology of diamondlike carbon and related materials: an updated review," *Surface and Coatings Technology*, vol. 94–95, pp. 507–513, Oct. 1997. doi:10.1016/S0257-8972(97)00458-1.

[6] X. R. Yan, T. Xu, S. S. Yue, H. W. Liu, Q. J. Xue and S. R. Yang, "Water repellency and surface free energy of a-C:H films prepared by heat treatment of polymer precursor," *Diamond and Related Mateirals*, vol. 14, iss. 8, pp. 1342–1347, Aug. 2005, doi:10.1016/j.diamond.2005.01.035.

[7] N. W. Khun, E. Liu, G. C. Yang, W. G. Ma and S. P. Jiang, "Structure and corrosion behavior of platinum/ruthenium/nitrogen doped diamond-like carbon thin films," *Journal of Applied Physics*, vol. 106, iss. 1, pp. 013506, Jul. 2009, doi:10.1063/1.3154022.

[8] H. Sun, L. Yang, H. Wu and L. Zhao, "Effects of element doping on the structure and properties of diamond-like carbon films: A review," *Lubricants*, vol. 11, iss. 4, pp. 186, Apr. 2023, doi: 10.3390/lubricants11040186.

[9] D. Bootkul, B. Supsermpol, N. Saenphinit, C. Aramwit and S. Intarasiri, "Nitrogen doping for adhesion improvement of DLC film deposited on Si substrate by filtered cathodic vacuum arc (FCVA) technique," *Applied Surface Science*, vol. 310, pp. 284–292, Aug. 2014, doi: 10.1016/j.apsusc.2014.03.059.

[10] H. Nakazawa, K. Nakamura, H. Osanai, Y. Sasaki, H. Koriyama, Y. Kobayashi, Y. Enta, Y. Suzuki and M. Suemitsu, "Annealing effects on the properties of hydrogenated diamond-like carbon films doped with silicon and nitrogen," *Diamond and Related Materials*, vol. 122, pp. 108809, Feb. 2022, doi:10.1016/j.diamond.2021.108809.

[11] Y. H. Lin, H. D. Lin, C. K. Liu, M. W. Huang, Y. C. Chen, J. R. Chen and H. C. Shih, "Annealing effect on the structural, mechanical, and electrical properties of titanium doped diamond-like carbon films," *Thin Solid Films*, vol. 518, iss. 5, pp. 1503–1507, Dec. 2009, doi.org/10.1016/j.tsf.2009.09.096.

[12] L. C. W. Richard, M. Kazuhisa, V. Rama and E. J. Howard, "Physical and tribological properties of rapid thermal annealed diamond-like carbon films," *Surface and Coatings Technology*, vol. 54–55, pp. 576-580, 1992, doi:10.1016/S0257-8972(07)80085-5.

[13] H. W. Choi, M. W. Moon, T. Y. Kim, K. R. Lee and K. H. Oh, "The thermal annealing effect on the residual stress and interface adhesion in the compressive stressed DLC film," *MRS Online Proceedings Library*, vol. 795, pp. 182–187, May 2003. doi:10.1557/PROC-795-U11.42.

[14] N. Konkhunthot, P. Photongkam, P. Wongpanya, "Improvement of thermal stability, adhesion strength, and corrosion performance of diamond-like carbon films with titanium doping," *Applied Surface Science*, vol. 469, pp. 471–486, Mar. 2019, doi:10.1016/j.apsusc.2018.11.028.

[15] Y. S. Yang and T. P. Cho, "Effect of annealing temperature on the water contact angle of PVD hard coatings," *Materials*, vol. 6, no. 8, pp. 3373–3386, Aug. 2013, doi.org: 10.3390/ma6083373.

[16] Q. Zhao, Z. Mou, B. Zhang, X. Zhang, Z. Wang, K. Wang and Q. Jia, "Revealing the corrosion resistance of amorphous carbon films under heat shocking via annealing," *Diamond and Related Materials*, vol. 102, pp. 107692, Feb. 2020, doi:10.1016/j.diamond.2019.107692.

[17] R. K. Vagapov, K. A. Ibatullin and D. N. Zapevalov, "Corrosion processes on steel under conditions of mositure condensation and in the presence of carbon dioxide," *Materials Science: Corrosion Protection*, vol. 56, pp. 673–680, Nov. 2020, doi.org: 10.1007/s10556-020-00825-5.

[18] N. W. Khun, E. Liu and X. T. Zeng, "Corrosion behavior of nitrogen doped diamond-like carbon thin films in NaCl solutions," *Corrosion Science*, vol. 51, iss. 9, pp. 2158–2164, Sep. 2009. doi:10.1016/j.corsci.2009.05.050.

[19] N. W. Khun and E. Liu, "Friction and wear of nitroen-doped DLC coating and platinum/ruthenium/nitrogen co-doped DLC nano-composite coatings," *Journal of Materials and Engineering*, vol. 3, iss. 1, pp. 67–77, 2025, doi: 10.61552/JME.2025.01.004.

[20] N. K. Manninen, R. E. Galindo, S. Carvalho and A. Cavaleiro, "Silver surface segregation in Ag-DLC nanocomposite coatings," *Surface and Coatings Technology*, vol. 267, pp. 90–97, Apr. 2015, doi:10.1016/j.surfcoat.2014.12.029.

[21] M. Cloutier, S. Turgeon, Y. Busby, M. Tatoulian, J. J. Pireaux and D. Mantovani, "Controlled distribution and clustering of silver in Ag-DLC nanocomposite coatings using a hybrid plasma approach," *ACS Applied Materials and Interfaces*, vol. 8, iss. 32, pp. 21020–21027, Jul. 2016, doi:10.1021/acsami.6b06614.

[22] R. K. Raman, A. K. Shukla, A. Gayen, M. S. Hegde, K. R. Priolkar, P. R. Sarode and S. Emura, "Tailoring a Pt-Ru catalyst for enhanced methanol electro-oxidation," *Journal of Power Source*, vol. 157, iss. 1, pp. 45–55, Jun. 2006. doi:10.1016/j.jpowsour.2005.06.031.

[23] S. C. Ray, W. Mbiombi and P. Papakonstantinou, "Diamond like carbon (DLC) thin films: preparation and characterization," *Applied Mechanics and Materials*, vol. 575, pp. 292–295, Jun. 2014. doi:10.4028/www.scientific.net/AMM.575.292.

[24] Y. Hayashi, K. M. Krishna, H. Ebisu, T. Soga, M. Umeno, T. Jimbo, "Optical and structural properties of nitrogen doped amorphous carbon films grown by rf plasma-enhanced CVD," *Diamond and Related Materials*, vol. 10, iss. 3–7, pp. 1002–1006, Jul. 2001, doi:10.1016/S0925-9635(00)00566-5.

[25] L. X. Liu and E. Liu, "Nitrogenated diamond-like carbon films for metal tracing," *Surface and Coatings Technology*, vol. 198, iss. 1-3, pp. 189–193, Aug. 2005, doi:10.1016/j.surfcoat.2004.10.031.

[26] J. T. Titantah and D. Lamoen, "Carbon and nitrogen 1s energy levels in amorphous carbon nitride systems: XPS interpretation using first-principles," *Diamond and Related Materials*, vol. 16, iss. 3, pp. 581–588, Mar. 2007, doi: 10.1016/j.diamond.2006.11.048.

[27] C. C. Chen, F. C. N. Hong, "Structure and properties of diamond-like carbon nao-composite films containing copper particles," *Applied Surface Science*, vol. 242, iss. 3–4, pp. 261–269, Apr. 2005, doi:10.1016/j.apsusc.2004.08.036.

[28] D. Beeman, J. Silverman, R. Lynds and M.R. Anderson, "Modeling studies of amorphous carbon," *Physical Review B*, vol. 30, iss. 2, pp. 870–875, 1984, doi: 10.1103/PhysRevB.30.870.

[29] C. S. Part, S. G. Choi, J. N. Jang, M. P. Hong, K. H. Kwon and H. H. Park, "Effect of boron and silicon doping on the surface and electrical properties of diamond like carbon films by magnetron sputtering technique," *Surface and Coatings Technology*, vol. 231, pp. 131–134, Sep. 2013, doi.org/10.1016/j.surfcoat.2012.01.014.

[30] L. Y. Chen and F. C. N. Hong, "Surface tension studies of (Si, N)-containing diamond-like carbon films deposited by hexamethyldisilazane," *Diamond and Related Materials*, vol. 12, iss. 3–7, pp. 968–973, Mar. 2003, doi:10.1016/S0925-9635(02)00351-5.

[31] M. Grischke, K. Bewilogua, K. Trojan and H. Dimigen, "Application oriented modifications of deposition processes for diamond-like carbon-based coatings," *Surface and Coatings Technology*, vol. 74–75, pp. 739–745, Oct. 1995, doi:10.1016/0257-8972(94)08201-4.

[32] H. K. Livingston and C. S. Swingley, "Contact angles in controlled atmospheres: Some theoretical considerations," *Surface Science*, vol. 24, iss. 2, pp. 625–634, Feb. 1971, doi:10.1016/0039-6028(71)90285-8.

[33] K. J. Kubiak, M. C. T. Wilson, T. G. Mathia and P. Carval, "Wettability versus roughness of engineering surfaces," *Wear*, vol. 271, iss. 3–4, pp. 523–528, Jun. 2011, doi: 10.1016/j.wear.2010.03.029

[34] D. Hill, H. Attia, A. R. Barron and S. Alexander, "Size and morphology dependent surface wetting based on hydrocarbon functionalized nanoparticles," *Journal of Colloid and Interface Science*, vol. 543, pp. 328–334, May 2019, doi: 10.1016/j.jcis.2019.02.058.

[35] L. Cao, J. Liu, Y. Wan and J. Pu, "Corrosion and tribocorrosion behavior of W doped DLC coating in artificial seawater," *Diamond and Related Materials*, vol. 109, pp. 108019, Nov. 2020, doi:10.1016/j.diamond.2020.108019.

[36] S. M. Fayed, D. Chen, S. Li, Y. Zhou, H. Wang and M. M. Sadawy, "Corrosion behavior and passive stability of multilayer DLC-Si coatings," *Surface and Coatings Technology*, vol. 431, pp. 128001, Feb. 2022, doi:10.1016/j.surfcoat.2021.128001.

[37] Y. Wang, K. Y. Li, F. Scenini, J. Jiao, S. J. Qu, Q. Luo and J. Shen, "The effect of residual stress on the electrochemical corrosion behavior of Fe based amorphous coatings in chloride containing solutions," *Surface and Coatings Technology*, vol. 302, pp. 27–38, Sep. 2016, doi:10.1016/j.surfcoat.2016.05.034.

[38] B. Tomcik, T. Osipowicz and J. Y. Lee, "Diamond-like films as a corroion protective layer on the hard disk," *Thin Solid Films*, vol. 360, iss. 1–2, pp. 173–180, Feb. 2000, doi:10.1016/S0040-6090(99)01093-7.

[39] L. Ru, Y. Wang, J. Liu, S. Tao and J. Xiao, "Hydrophobic, anticorrosion, and frictional properties of F-DLC films prepared by magnetron sputtering," *Vacuum*, vol. 217. pp. 112567, Nov. 2023, doi:10.1016/j.vacuum.2023.112567.

[40] R. Braak, U. May, L. Onuseit, G. Repphun, M. Guenther, C. Schmid and K. Durst, "Accelerated thermal degradation of DLC coatings via growth defects," *Surface and Coatings Technology*, vol. 349, pp. 272–278, Sep. 2018. doi:10.1016/j.surfcoat.2018.05.063.

[41] L. Wang, X. Nie and X. Hu, "Effect of thermal annealing on tribological and corrosion properties of DLC coatings," *Journal of Materials Engineering and Performance*, vol. 22, iss. 10, pp. 3093–3100, Oct. 2013. doi:10.1007/s11665-013-0585-0.

[42] W. Zhang, Y. Xia, J. Ju, L. Wang, Z. Fang and M. Zhang, "Electrical conductivity of nitirde carbon films with different nitrogen content," *Solid State Communications*, vol. 126, iss. 3, pp. 163–166, Apr. 2003, doi:10.1016/S0038-1098(02)00673-7.

[43] F. R. Marciano, E. C. Almeida, D. A. L. Oliveira, E. J. Corat and V. J. T. Airoldi, "Improvement of DLC electrochemical corrosion resistance by addiction of fluorine," *Diamond and Related Materials*, vol. 19, iss. 5–6, pp. 537–540, May 2010, doi:10.1016/j.diamond.2009.12.015.